Atomic Layer Processing of MoS_2

John D. Hues, Jacob A. Tenorio, Icelene Leong, Steven M. Hues, Elton Graugnard*
Micron School of Material Science and Engineering,
Boise State University, 1910 University Dr., Boise, ID, USA 83725

ABSTRACT

Two-dimensional materials, including transition metal dichalcogenides (TMDs), have attracted attention for potential use in electronic, photonic, and optoelectronic applications. Molybdenum disulfide (MoS_2) is a widely studied TMD that offers potential for improving speed and efficiency in scaled electronic devices. However, advancing MoS_2 and other 2D materials into high volume device manufacturing requires scalable deposition and etching processes that are compatible with manufacturing constraints. Atomic layer deposition (ALD) and atomic layer etching (ALE) are scalable deposition processes that deposit and etch films at relatively low temperatures. Together, atomic layer deposition and atomic layer etching constitute complementary facets of atomic layer processing. Here, we report progress in combining thermal ALD and thermal ALE of MoS_2 followed by annealing to produce crystalline few-layer films. Combining the two processes offers greater control over film uniformity and thickness. Using ALD at 200 °C with MoF_6 and H_2S followed by ALE at 200 °C with MoF_6 and H_2O and post-deposition annealing in H_2S, we achieved few-layer MoS_2 films as assessed by the separation of the characteristic Raman modes of MoS_2. Using analysis of the Raman spectra for indirect assessment of defect concentrations allowed correlation of the annealing conditions to the quality of the MoS_2 films for accelerated process development. These combined thermal processes and the promising results represent progress towards the integration of MoS_2 films into device manufacturing.

Keywords: Atomic layer deposition, atomic layer etching, 2D materials, molybdenum disulfide

1. INTRODUCTION

Two-dimensional (2D) materials, and particularly 2D transition metal dichalcogenides (TMDs), such as molybdenum disulfide (MoS_2), are prime candidates to replace components in silicon (Si) microelectronic device nodes when dimensions (e.g., channel thickness) scale to the point where Si properties degrade.[1] However, the scalable synthesis of 2D materials faces significant challenges, and the measured properties of 2D materials often fall short of their predicted values.[2] Integrating 2D materials into manufacturing requires control of layer number (thickness), thickness uniformity, defect density, dielectric interface quality, contact resistance, and more.[3] Chemical vapor deposition (CVD) has been used to produce high quality 2D TMDs, but requires high temperatures or the use of seeding promoters.[4, 5] A variant of CVD, atomic layer deposition (ALD) uses self-limiting surface reactions to deposit thin films in a precise layer-by-layer manner.[6] The nature of ALD allows use of highly reactive chemical precursors, which enables deposition at low temperatures, but in the case of TMDs, the resulting films are amorphous or nanocrystalline.[7] Further, since deposition is controlled by surface reactions, the deposition temperature and surface chemistry control the density of reaction sites, film uniformity, grain size, film morphology, and phase.[8] Post-deposition annealing (PDA) can be used to control the crystallinity and phase of a deposited film.[8] Additionally, to improve film uniformity, deposition and etch-back processes have been developed and shown to reduce surface roughness and ensure film coalescence.[9]

In the case of ALD of MoS_2 with MoF_6 and H_2S, deposition at 200 °C and below results in amorphous films that crystallize into a layered 2H structure during annealing.[10, 11] The annealing temperature and environment strongly influence the atomic coordination and film quality.[11] To further explore strategies for improving MoS_2 quality, we explored the impact of annealing temperatures and implemented a deposition, etch-back, and anneal process. Here, we report progress in employing each of these strategies for deposition of uniform few-layer MoS_2 films with quality approaching CVD levels.

*eltongraugnard@boisestate.edu; atomicfilmslab.org

Low-Dimensional Materials and Devices 2024, edited by Nobuhiko P. Kobayashi, A. Alec Talin, Albert V. Davydov, M. Saif Islam, Proc. of SPIE Vol. 13114, 131140A
 · 0277-786X · doi: 10.1117/12.3028874

2. METHODOLOGY

ALD, ALE, and PDA processes were performed in a custom tube-furnace based reactor. The reactor operates in viscous flow during deposition and etching but was held static during annealing. To promote nucleation, Si(100) coupons were first coated with 5 nm of alumina via ALD with trimethylaluminum and water (H_2O) at 200 °C. The alumina coating yields a surface with a high hydroxyl concentration, which promotes the dissociative adsorption of MoF_6.[12, 13] Without removing the samples from the vacuum chamber, amorphous MoS_x films were deposited at 200 °C using 20 cycles of molybdenum hexafluoride (MoF_6) and hydrogen sulfide (H_2S). Etch-back was then performed with varying cycles of ALE at 200 °C using MoF_6 and H_2O. Details of the ALD and ALE processes have been reported previously.[10, 14] Following the etch-back, the samples were annealed at 900 °C in ~2 Torr of H_2S/N_2 (roughly 1.5 Torr H_2S partial pressure) for 60 minutes. Following the anneal, the reactor was cooled to <100 °C before removing the samples.

Post anneal, the samples were characterized ex situ using X-ray photoelectron spectroscopy (XPS) and Raman spectroscopy. XPS measurements were performed using a Physical Electronics (PHI) 5600 ESCA system using a monochromated Al K-alpha source with an analysis area of 3 mm × 10 mm. Survey scans used a pass energy of 200 eV and step size of 1 eV. High resolution scans used a pass energy of 50 eV and step size of 0.1 eV. The XPS data were analyzed using MultiPak 9.6. All spectra were referenced to the 1s peak (284.8 eV) of adventitious carbon. Peak fitting of all high-resolution scans utilized an iterated Shirley background to define the baseline. Region bounds were chosen such that bounds encompassed the totality of peaks present and were extended as far as possible without overlapping with other chemical peaks nearby. A Gaussian-Lorentzian peak mix was used when fitting spectra. Deconvolved spectra were used to determine the stoichiometry of the films using the assigned MoS_2 contributions following previous studies.[13]

Raman spectroscopy was conducted on a Horiba LabRAM system in reflection mode. A 532 nm excitation laser, using a 100× aperture was used to probe samples. A neutral density filter setting at 10% was used to prevent damage to the MoS_2 samples. Spectra were acquired over the 360-440 cm^{-1} range to capture crystalline MoS_2 modes. Peak fitting using Voigt functions was used analyze the Raman spectra and separate the contributions from the crystalline (E^1_{2g} and A_{1g}) and defect-induced modes and to extract the center wavenumbers of the modes, similar to previous studies of MoS_2.[15]

3. RESULTS AND DISCUSSION

Raman Spectroscopy

Raman spectra for the deposition-etch-anneal (DEA) samples are shown in Fig. 1. The characteristic E^1_{2g} (~384 cm^{-1}) and A_{1g} (406 cm^{-1}) modes are observed with mode intensities highest for the thicker films (10 ALE etch-back cycles) versus the thinner films (40 ALE cycles). The characteristic spectra also contain contributions from defect-related phonon modes,[15] and peak fitting was used to separate contributions of the defect modes from the E^1_{2g} and A_{1g} modes. Based on the peak positions extracted during peak fitting, the characteristic mode spacing, which can be related to the number of MoS_2 layers, becomes smaller with increasing numbers of ALE cycles. Extracted peak positions and mode spacings are provided in Table 1. Following 30 ALE cycles, the mode spacing is 21 cm^{-1}, consistent with roughly 2 MoS_2 layers.[16] However, after 40 ALE cycles, the mode spacing did not decrease further (a spacing of ~17-19 cm^{-1} would be expected for monolayer MoS_2). The peak separations are plotted versus cycle number in Figure. 2a. A clear trend in decreasing peak separation versus cycle number is observed for 10-30 cycles. However, the trend does not continue to 40 ALE cycles, which yielded roughly the same peak separation as 30 ALE cycles. For amorphous MoS_x, the deposition rate on alumina at 200 °C is ~2 Å/cycle,[13] while the etch rate at 200 °C is 0.5 Å/cycle.[14] Based on these estimates, the process with 20 ALD and 40 ALE cycles should result in an amorphous film thickness of ~20 Å. However, a volume reduction of ~40% was observed previously during annealing at 650 °C. Thus, following the 40 ALE cycles and PDA at 900 °C, it is reasonable to expect a film thickness of ~12 Å, which is greater than the ~7 Å thickness for monolayer MoS_2.

The lack of a further reduction in the spacing between the characteristic Raman modes may be the results of etch-stop behavior or could reflect an elevated defect density within the film. In prior studies of the ALE process,[14] etch-stop behavior consisting of a slowing etch per cycle was observed as the etching progressed toward the film substrate interface. This behavior is not yet understood but is attributed to the complex surface reactions involved in transitioning from nucleation reactions on the alumina surface to growth reactions of the MoS_x film.

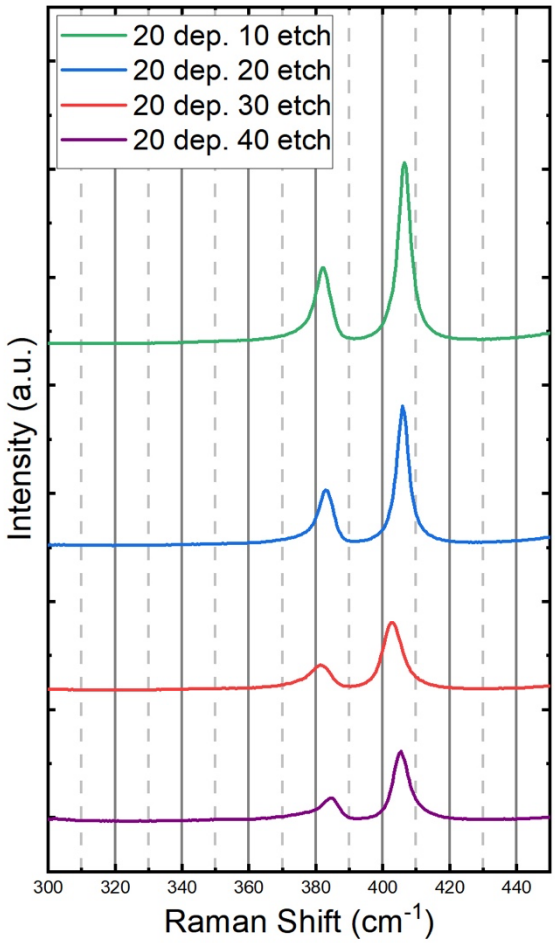

Figure 1. Raman spectra for MoS_2 films deposited through a deposition-etch-anneal process. All films were deposited at 200 °C with 20 cycles of ALD using MoF_6 and H_2S. Various numbers of ALE cycles were then performed at 200 °C using MoF_6 and H_2O. Samples were then annealed at 900 °C for 60 minutes in ~2 Torr of H_2S/N_2. Characteristic peaks observed near 382 cm^{-1} are assigned to the in-plane E^1_{2g} mode and those near 405 cm^{-1} are assigned to the out-of-plane A_{1g} mode. Values of the peak are listed in Table 1. Peak intensity and separation between peaks decrease with increasing ALE cycle number.

Table 1. Positions and spacings between characteristic Raman modes for MoS_2 films following the deposition-etch-anneal process. Values and standard deviations were determined through peak fitting.

Etch Cycles	E^1_{2g} Position (cm^{-1})	A_{1g} Position (cm^{-1})	Peak Separation (cm^{-1})
10	382.26 ± 0.03	406.489 ± 0.007	24.23 ± 0.04
20	383.13 ± 0.02	405.972 ± 0.008	22.85 ± 0.03
30	381.68 ± 0.03	402.745 ± 0.009	21.06 ± 0.04
40	384.56 ± 0.04	405.267 ± 0.007	20.70 ± 0.05

Alternately, prior work has shown that defect densities about ~5×10^{12} cm^{-2} result in an increased mode spacing for monolayer MoS_2.[15] To further assess the defect densities within the films, we analyzed the E^1_{2g} region and decomposed the peak into the E^1_{2g} peak and a defect-induced shoulder at lower Raman shift that broadens the apparent peak width. The defect-related mode is assigned to a transverse optical (TO) branch of the phonon spectrum at the *M* point,[15] and its magnitude reflects the defect density of the film. In Fig. 2b, we plot the ratio of the peak areas for the shoulder (TO(*M*)) and E^1_{2g} peaks. For 10, 20, and 30 ALE cycles, the ratio is between 0.2 to 0.3 but increases to nearly 0.6 for the 40 ALE cycle sample. Note, a ratio of ~0.1 is expected for CVD quality films with lower defect densities. These data support the

conclusion that there is an increased defect density for the sample that underwent 40 ALE cycles. Additional structural characterization is required to understand the defect densities within the DEA films and to gain insights into the structural transitions occurring during annealing of the ultrathin films.

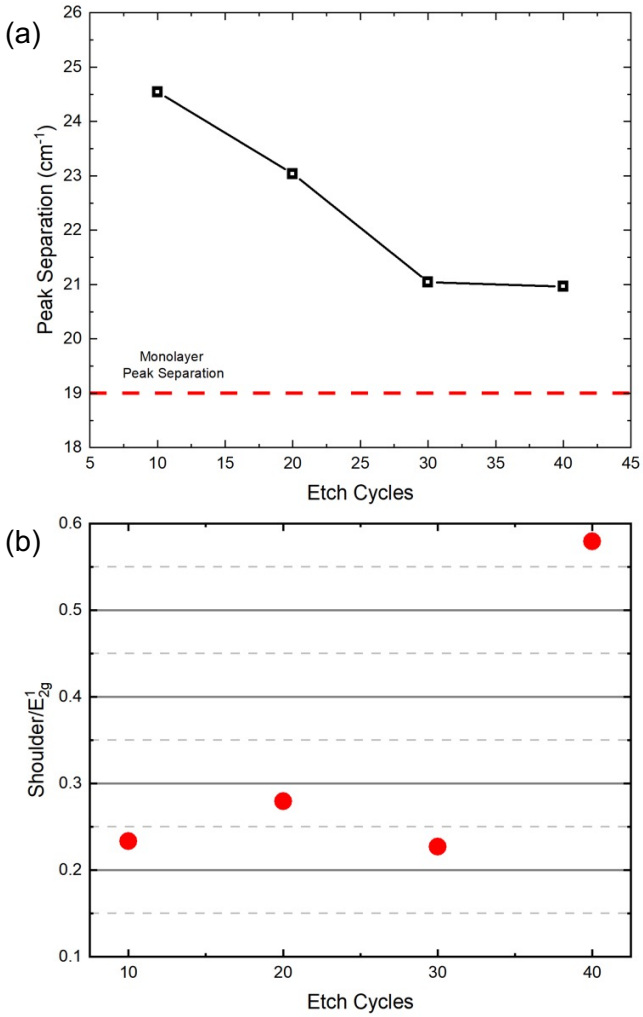

Figure 2. Analysis of Raman spectra for deposition-etch-anneal MoS_2 samples. (a) A plot of peak separation between the fitted values of the E^1_{2g} and A_{1g} modes of MoS_2 (values provided in Table 1). The peak separation decreases with increasing number of pre-anneal ALE cycles for 10 to 30 cycles, but the trend does not continue to 40 cycles, which exhibited a separation of ~21 cm^{-1}, roughly equal to that at 30 cycles. (b) A plot of the ratio of the areas for the fitted TO(*M*) shoulder peak and E^1_{2g} peak versus cycle number. Lower ratios are consistent with lower defect densities within the films. A sharp increase in the ratio is observed for the sample that underwent 40 ALE cycles.

X-ray Photoelectron Spectroscopy

To further characterize the MoS_2 films, high-resolution XPS spectra were acquired for samples annealed at 900 °C in ~2 Torr H_2S for 60 minutes following 20 and 30 ALE cycles. The spectra, shown in Fig. 3, were analyzed to determine the contributions of Mo-S and Mo-O bonding and estimate the S:Mo ratio. The higher amount of Mo-O bonding observed in the 30 ALE cycles sample may result from the thinner films revealing a stronger contribution from the Mo-O bonding at the alumina substrate surface. Nonetheless, for both samples, the S:Mo ratio was found to be 1.6, which is somewhat low indicating a sulfur-deficient film despite the high H_2S partial pressure during annealing. Additional work is required

to establish the relationship between H_2S partial pressure, annealing time and temperature, and the resulting film stoichiometry. Also, XPS spectra of the 40 ALE cycle sample may provide additional insights into the defects within that film.

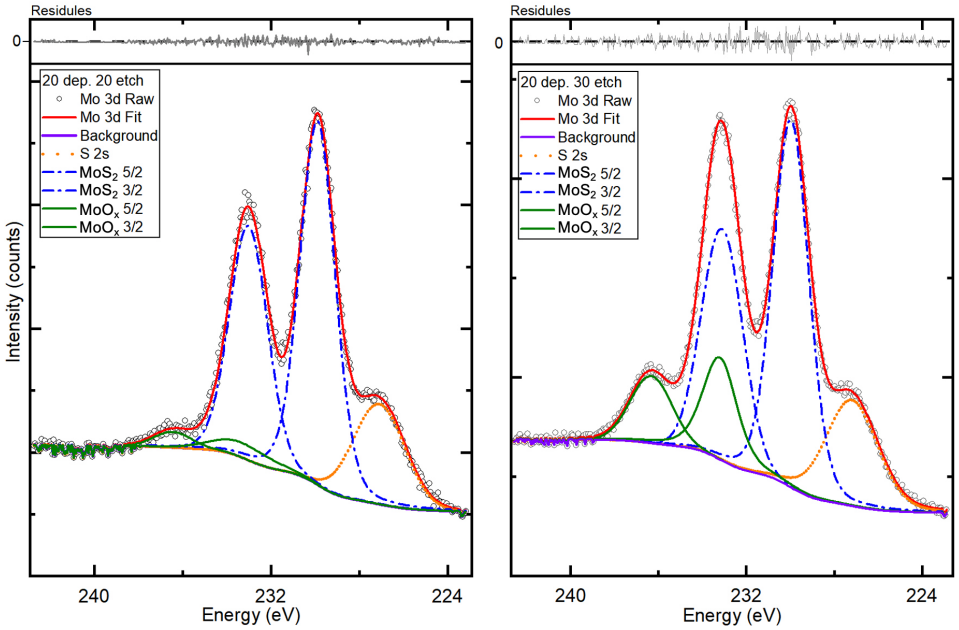

Figure 3. High-resolution X-ray photoelectron spectra of the Mo 3d region for MoS_2 films following the deposition-etch-anneal process. Each film was deposited using 20 cycles of ALD followed immediately by ALE, both at 200 °C. Samples were then annealed at 900 °C in ~2 Torr of H_2S/N_2 for 60 min. The number of ALE cycles is shown for each spectrum: (a) 20 cycles and (b) 30 cycles. Peak fitting was performed to determine the relative amounts of Mo-S and Mo-O bonding. The decomposed spectral assignments are shown in the figure legends.

4. SUMMARY

Preliminary results for atomic layer processing of few-layer MoS_2 films using a deposition-etch-anneal (DEA) process were reported. The DEA process with increasing cycles of atomic layer etching produced films with decreasing thickness, as assessed using the separation of the characteristic Raman modes of MoS_2. Deviation from the trend of decreasing peak separation with increasing ALE cycle number was observed and is attributed to a decreasing etch per cycle as the film thickness approached the transitionary nucleation interface between the MoS_2 and underlying alumina substrate surface. Raman spectra were further analyzed to quantify the defect densities within the films and revealed a sharp decrease for the thinnest DEA films, which may again reflect process complexity in the vicinity of the nucleation interface. XPS analysis revealed that the films were sub-stoichiometric despite annealing in a H_2S rich environment. Additional work is necessary to understand the atomic structures of the films, the nature of the defects, and the true film thicknesses and layer numbers. However, the results support atomic layer processing as a powerful approach to scalable synthesis of few layer MoS_2 films.

ACKNOWLEDGEMENTS

This work was supported in part by Department of Energy AMMTO, the National Science Foundation Center for Atomically Thin Multifunctional Coatings (ATOMIC) IUCRC (grant no. 2113873), and Semiconductor Research Corporation (SRC) and DARPA.

REFERENCES

[1] Brien, K. P. O.; Dorow, C. J.; Penumatcha, A.; Maxey, K.; Lee, S.; Naylor, C. H.; Hsiao, A.; Holybee, B.; Rogan, C.; Adams, D.; et al. Advancing 2D Monolayer CMOS Through Contact, Channel and Interface Engineering. In *2021 IEEE International Electron Devices Meeting (IEDM)*, 11-16 Dec. 2021, 2021; pp 7.1.1-7.1.4. DOI: 10.1109/IEDM19574.2021.9720651.

[2] Yin, L.; Cheng, R.; Ding, J.; Jiang, J.; Hou, Y.; Feng, X.; Wen, Y.; He, J. Two-Dimensional Semiconductors and Transistors for Future Integrated Circuits. *ACS Nano* **2024**, *18* (11), 7739-7768. DOI: 10.1021/acsnano.3c10900.

[3] Das, S.; Sebastian, A.; Pop, E.; McClellan, C. J.; Franklin, A. D.; Grasser, T.; Knobloch, T.; Illarionov, Y.; Penumatcha, A. V.; Appenzeller, J.; et al. Transistors based on two-dimensional materials for future integrated circuits. *Nature Electronics* **2021**, *4* (11), 786-799. DOI: 10.1038/s41928-021-00670-1.

[4] Lei, Y.; Zhang, T.; Lin, Y.-C.; Granzier-Nakajima, T.; Bepete, G.; Kowalczyk, D. A.; Lin, Z.; Zhou, D.; Schranghamer, T. F.; Dodda, A.; et al. Graphene and Beyond: Recent Advances in Two-Dimensional Materials Synthesis, Properties, and Devices. *ACS Nanoscience Au* **2022**, *2* (6), 450-485. DOI: 10.1021/acsnanoscienceau.2c00017.

[5] Zhu, J.; Park, J.-H.; Vitale, S. A.; Ge, W.; Jung, G. S.; Wang, J.; Mohamed, M.; Zhang, T.; Ashok, M.; Xue, M.; et al. Low-thermal-budget synthesis of monolayer molybdenum disulfide for silicon back-end-of-line integration on a 200 mm platform. *Nat. Nanotechnol.* **2023**, *18* (5), 456-463. DOI: 10.1038/s41565-023-01375-6.

[6] George, S. M. Atomic Layer Deposition: An Overview. *Chem. Rev.* **2010**, *110* (1), 111-131. DOI: 10.1021/cr900056b.

[7] Mattinen, M.; Leskelä, M.; Ritala, M. Atomic Layer Deposition of 2D Metal Dichalcogenides for Electronics, Catalysis, Energy Storage, and Beyond. *Adv. Mater. Interfaces* **2021**, *8* (6), 2001677. DOI: https://doi.org/10.1002/admi.202001677.

[8] Miikkulainen, V.; Leskelä, M.; Ritala, M.; Puurunen, R. L. Crystallinity of inorganic films grown by atomic layer deposition: Overview and general trends. *J. Appl. Phys.* **2013**, *113* (2). DOI: 10.1063/1.4757907.

[9] Gerritsen, S. H.; Chittock, N. J.; Vandalon, V.; Verheijen, M. A.; Knoops, H. C. M.; Kessels, W. M. M.; Mackus, A. J. M. Surface Smoothing by Atomic Layer Deposition and Etching for the Fabrication of Nanodevices. *ACS Appl. Nano Mater.* **2022**, *5* (12), 18116-18126. DOI: 10.1021/acsanm.2c04025.

[10] Mane, A. U.; Letourneau, S.; Mandia, D. J.; Liu, J.; Libera, J. A.; Lei, Y.; Peng, Q.; Graugnard, E.; Elam, J. W. Atomic layer deposition of molybdenum disulfide films using MoF_6 and H_2S. *J. Vac. Sci. Technol. A* **2018**, *36* (1). DOI: 10.1116/1.5003423.

[11] Letourneau, S.; Young, M. J.; Bedford, N. M.; Ren, Y.; Yanguas-Gil, A.; Mane, A. U.; Elam, J. W.; Graugnard, E. Structural evolution of molybdenum disulfide prepared by atomic layer deposition for realization of large scale films in microelectronic applications. *ACS Appl. Nano Mater.* **2018**, *1* (8), 4028-4037.

[12] Lawson, M.; Graugnard, E.; Li, L. First-principles studies of MoF_6 absorption on hydroxylated and non-hydroxylated metal oxide surfaces and implications for atomic layer deposition of MoS_2. *Appl. Surf. Sci.* **2021**, *541*, 148461.

[13] Soares, J.; Letourneau, S.; Lawson, M.; Mane, A. U.; Lu, Y.; Wu, Y.; Hues, S. M.; Li, L.; Elam, J. W.; Graugnard, E. Nucleation and growth of molybdenum disulfide grown by thermal atomic layer deposition on metal oxides. *J. Vac. Sci. Technol. A* **2022**, *40* (6), 062202. DOI: 10.1116/6.0002024.

[14] Soares, J.; Mane, A. U.; Choudhury, D.; Letourneau, S.; Hues, S. M.; Elam, J. W.; Graugnard, E. Thermal Atomic Layer Etching of MoS_2 Using MoF_6 and H_2O. *Chem. Mater.* **2023**, *35* (3), 927–936. DOI: 10.1021/acs.chemmater.2c02549.

[15] Mignuzzi, S.; Pollard, A. J.; Bonini, N.; Brennan, B.; Gilmore, I. S.; Pimenta, M. A.; Richards, D.; Roy, D. Effect of disorder on Raman scattering of single-layer $\mathrm{Mo}{\mathrm{S}}_{2}$. *Physical Review B* **2015**, *91* (19), 195411. DOI: 10.1103/PhysRevB.91.195411.

[16] Zhang, X.; Qiao, X.-F.; Shi, W.; Wu, J.-B.; Jiang, D.-S.; Tan, P.-H. Phonon and Raman scattering of two-dimensional transition metal dichalcogenides from monolayer, multilayer to bulk material. *Chemical Society Reviews* **2015**, *44* (9), 2757-2785. DOI: 10.1039/C4CS00282B.